Ordering of oblate hard particles between symmetric penetrable walls

TEIXEIRA, PIC <http://orcid.org/0000-0003-2315-2261>, ANQUETIL-DECK, C <http://orcid.org/0000-0003-2444-125X> and CLEAVER, Doug <http://orcid.org/0000-0002-4278-0098>

Ordering of oblate hard particles between symmetric penetrable walls

P. I. C. Teixeira*

ISEL – Instituto Superior de Engenharia de Lisboa, Instituto Politécnico de Lisboa

Rua Conselheiro Emídio Navarro 1, 1959-007 Lisboa, Portugal and

Centro de Física Teórica e Computacional, Faculdade de Ciências,

Universidade de Lisboa, 1749-016 Lisboa, Portugal

C. Anquetil-Deck†

Department of Chemical Engineering,

Norwegian University of Science and Technology,

Sem Sælandsvei 4, NO–7491 Trondheim, Norway

D. J. Cleaver‡

Materials and Engineering Research Institute, Sheffield Hallam University

Pond Street, Sheffield S1 1WB, United Kingdom

(Dated: 1 May 2020)

Abstract

We find the structure of a model discotic liquid crystal (DLC) confined between symmetric walls of controllable penetrability. The model consists of oblate hard Gaussian overlap (HGO) particles. Particle-substrate interactions are modelled as follows: each substrate sees a particle as a disc of zero thickness and diameter D less than or equal to that of the actual particle, σ_0, embedded inside the particle and located halfway along, and perpendicular to, its minor axis. This allows us to control the anchoring properties of the substrates, from planar (edge-on) for $D \sim 0$ to homeotropic (face-on) for $D \sim \sigma_0$. This system is investigated using both Monte Carlo simulation and density-functional theory, the latter implemented at the level of Onsager's second-virial approximation with Parsons-Lee rescaling. We find that the agreement between theory and simulation is substantially less good than for prolate HGOs; in particular, the crossover from edge-on to face-on alignment is predicted by theory to occur at $D \sim 0.65\sigma_0$, but simulation finds it for $D \sim 0.55\sigma_0$. These discrepancies are likely a consequence of the fact that Onsager's theory is less accurate for discs than for rods. We quantify this by computing the bulk isotropic-nematic phase diagram of oblate HGOs.

Liquid crystal films; anchoring transitions; density-functional theory; Monte Carlo simulation

*Electronic address: piteixeira@fc.ul.pt

†Electronic address: candy.deck@ntnu.no

‡Electronic address: D.J.Cleaver@shu.ac.uk

I. INTRODUCTION

Liquid crystal (LC) devices (LCDs) are now literally in every pocket: indeed, they have become so common we hardly notice them anymore. All current LCDs rely, for their operation, on the competing actions of bounding surfaces, known as anchoring, and of applied fields on the preferred orientation of the particles making up the LC. The fundamental problem at the heart of LC applications is to understand how a given bounding surface modifies the properties of a given LC to induce a resultant alignment. Most theoretical and simulation-based studies on confined LCs to date have focused on rod-like particles, such as hard ellipsoids (HEs) [1, 2] or hard spherocylinders (HSCs) [3–5]. This reflects the fact that the traditional building blocks of LC phases are elongated objects, either at the molecular or colloidal level [6]. However, it is now possible to synthesise a huge variety of molecular shapes, including plates and discs [7]. Such discotic LCs (DLCs) are also realised in colloidal dispersions, e.g., of gibbsite [8] or clay [9] particles. DLCs may exhibit semiconducting properties, with promising applications in the photovoltaic industry [10]. They are also effective as lubricants, outperforming hydrocarbons in some conditions [11]. This, as well as sheer curiosity, has spawned a number of theoretical, computational and experimental studies of DLCs at surfaces and interfaces.

Harnau and Dietrich used extensions of Onsager's second-virial theory to study infinitely-thin hard discs with continuous orientations [12] and binary mixtures of hard platelets with restricted orientations [13], at a hard wall. They found that (face-on) ordering effects are significant already at fairly low densities. Schmidt and co-workers developed a fundamental-measure (FM) density-functional theory (DFT) of infinitely thin hard platelets, both pure and mixed [14]. They then applied this to the isotropic-nematic (I–N) interface of suspensions of colloidal platelets [15, 16], with results superior to those of Onsager's second-virial theory. They also investigated the capillary nematisation of thin hard discs between parallel hard walls, and concluded that the I–N transition of plates is suppressed much less strongly by confinement than that of rods [17]. More recently, Kapanowski and Abram [18] found, on the basis of Onsager's second-virial theory, that hard platelets prefer to lie flat at a hard wall and will order biaxially only if the bulk phase itself is biaxial.

On the *in silico* front, Piñeiro *et al.* [19] have performed NPT and Gibbs ensemble Monte Carlo (MC) simulations of hard cut spheres of aspect ratio $L/D = 0.1$ in a slab geometry,

between either hard walls that exclude the particles completely, or adsorbent walls that exclude only the particles' centres-of-mass. Hard walls were revealed to induce homeotropic (face-on) anchoring and stabilise the N phase, whereas adsorbent walls promoted planar (edge-on) alignment and a more disordered bulk. Avendaño *et al.* [20] have reported what is, to our knowledge, the only computer simulation of a non-convex DLC composed of soft-repulsive rings between parallel, soft-repulsive walls. These tend to align edge-on, forming low-density smectic layers with anti-nematic order and no biaxiality, in stark contrast to the behaviour of convex DLCs. Finally, other numerical studies of confined DLCs have employed the popular Gay-Berne (GB) model and more complex wall-particle interactions [21–25].

In spite of all the above, more work is needed to establish the design principles for DLCs in confined environments. In particular, we are missing a simple, preferably (for ease of use and generality) hard-body, model that would allow one to switch between different types of anchoring in either symmetric or hybrid systems, by tuning a physically transparent parameter. Our purpose here is to develop such a model and interrogate how effective DFT and MC simulation are at representing the range of behaviours accessible to such systems. This will then provide foundations for potentially more ambitious investigations involving more sophisticated combinations of substrates and model mesogens.

This paper is organised as follows: in section II we summarise our model and theory, which have been described in detail in previous papers. Section III gives details of the computer simulations performed to validate our calculations. Results from theory and simulation are then compared in section IV. Finally we conclude in section V.

II. THEORY

As in earlier work [26, 28–30], we consider a purely steric microscopic model of uniaxial particles represented by the hard Gaussian overlap (HGO) potential [31]. but which are now disc-shaped, i.e., of length-to-breadth ratio $\kappa = \sigma_L/\sigma_0 < 1$. For moderate κ, the HGO particles are a good approximation to hard ellipsoids (HEs) [32–34]; furthermore, their virial coefficients (and thus their equations of state, at least at low to moderate densities) are very similar [35, 36]. From a computational point of view, HGOs have the considerable advantage over HEs that the distance of closest approach between two particles is given in closed form [37]. Particle–substrate interactions are now modelled, as in [17], by a hard disc–wall (HDW)

potential (see figure 1):

$$\beta\mathcal{V}^{HDW}(z,\theta) = \begin{cases} 0 & \text{if } |z - z_0^\alpha| \geq \frac{1}{2}D\sin\theta \\ \infty & \text{if } |z - z_0^\alpha| < \frac{1}{2}D\sin\theta \end{cases} \tag{1}$$

where $\beta = 1/k_{\mathrm{B}}T$ and the z-axis has been chosen to be perpendicular to the substrates, located at $z = z_0^\alpha$ ($\alpha = 1, 2$). According to equation (1), particles see each other as HGOs, but the substrates see a particle as an infinitely thin disc of diameter D (which need not be the same at both substrates, or in different regions of each substrate [38, 39]). This is the oblate-particle version of the hard needle-wall potential of our earlier work [27–30]: physically, $0 < D < \sigma_0$ means that the particles are able to embed their side- and end groups, but not the whole width of their cores, into the bounding walls. In an experimental situation, this might be achieved by manipulating the density, orientation or chemical affinity of an adsorbed surface layer. In what follows, the substrate is characterised using the dimensionless parameter $D_s = D/\sigma_0$; as shown in [27, 28], this allows us to set the anchoring at either wall as either homeotropic (face-on) for $D_s \lesssim 1$, or planar degenerate (edge-on) for $D_s \ll 1$), although anchoring *strengths* cannot be finely controlled thus.

Because, for unpatterned substrates, the HDW interaction only depends on z and θ, it is reasonable to assume that there is no in-plane structure, so that all quantities are functions of z only. The grand-canonical functional [40] of an HGO film of bulk (i.e., overall) number density ρ at temperature T is then written, in our usual approximations [26, 28–30],

$$\begin{aligned} \frac{\beta\Omega\left[\rho(z,\omega)\right]}{S_{xy}} &= \int \rho(z,\omega)\left[\log\rho(z,\omega) - 1\right]\, dzd\omega \\ &\quad - \frac{\left(1 - \frac{3}{4}\xi\right)\xi}{2(1-\xi)^2}\int \rho(z_1,\omega_1)\Xi(z_1,\omega_1,z_2,\omega_2)\rho(z_2,\omega_2)\, dz_1 d\omega_1 dz_2 d\omega_2 \\ &\quad + \beta\int\left[\sum_{\alpha=1}^{2}\mathcal{V}^{HDW}(|z - z_0^\alpha|,\theta) - \mu\right]\rho(z,\omega)\, dzd\omega, \end{aligned} \tag{2}$$

where $\omega_i = (\theta_i, \phi_i)$ denote the polar and azimuthal angles describing the orientation of the long axis of a particle, S_{xy} is the interfacial area, μ is the chemical potential, $\xi = \rho v_0 = (\pi/6)\kappa\rho\sigma_0^3$ is the bulk packing fraction, $\Xi(z_1,\omega_1,z_2,\omega_2)$ is the area of a slice (cut parallel to the bounding plates) of the excluded volume of two HGO particles of orientations ω_1 and ω_2 and centres at z_1 and z_2 [41], for which an analytical expression has been derived [37]. $\rho(z,\omega)$ is the density-orientation profile in the presence of the external potential $\mathcal{V}^{HNW}(z,\theta)$: it is related to the probability that a particle positioned at z has orientation between ω and $\omega + d\omega$.

Three remarks are in order. Firstly, note that each surface particle experiences an environment that has both polar *and* azimuthal anisotropy, as a consequence of the excluded-volume interactions between the particles in addition to the 'bare' wall potential. Secondly, because we are dealing with hard-body interactions only, for which the temperature is an irrelevant variable, we can set $\beta = 1/k_{\mathrm{B}}T = 1$ in all practical calculations (it is retained in the formulae for generality). Thirdly, and finally, the prefactor multiplying the second integral in equation (2) is a simplified implementation of the Parsons-Lee density re-scaling [42, 43], which amounts to (approximately) summing the higher virial coefficients. In the spirit of [44, 45], this prefactor is a function of the *bulk* density, and not of the *local* density, which should be valid provided the density does not exhibit sharp spatial variations. Equation (2) is therefore the 'corrected' Onsager approximation to the free energy of the confined HGO fluid, which is expected to perform better for particle elongations $\kappa \ll \infty$ to the extent that structure is determined by location in the phase diagram. However, because this is a simple re-scaling of the density, no new structure that is not captured by the Onsager approximation is expected. More sophisticated approaches exist (see, e.g.,[46, 47]), but the purpose here, as stated above, is to look at the qualitative features of phenomena arising in the vicinity of the I–N transition of oblate hard particles, so the simplest possible microscopic treatment of anchoring is used that yields fairly good results for prolate HGOs [26, 28–30].

From minimisation of the grand canonical functional, equation (2),

$$\frac{\delta\Omega\left[\rho(z,\omega)\right]}{\delta\rho(z,\omega)} = 0, \tag{3}$$

we obtain the Euler-Lagrange equation for the equilibrium density-orientation profile,

$$\log\rho(z,\omega) = \beta\mu - \frac{\left(1-\frac{3}{4}\xi\right)}{\left(1-\xi\right)^2}\int' \Xi(z,\omega,z',\omega')\rho(z',\omega')\,dz'd\omega', \tag{4}$$

where the effect of the wall potentials, given by equation (1), has been incorporated through restriction of the range of integration over θ:

$$\int' d\omega = \int_0^{2\pi} d\phi \int_{\pi-\theta_m}^{\theta_m} \sin\theta\, d\theta = \int_0^{2\pi} d\phi \int_{-\cos\theta_m}^{\cos\theta_m} dx, \tag{5}$$

with

$$\sin\theta_m = \begin{cases} 1 & \text{if } |z-z_0^\alpha| \geq \frac{D}{2} \\ \frac{|z-z_0|}{D/2} & \text{if } |z-z_0^\alpha| < \frac{D}{2} \end{cases}, \tag{6}$$

z_0^α being, we recall, the position of substrate α.

Once $\rho(\omega, z)$ has been found, we can integrate out the angular dependence to get the density profile,

$$\rho(z) = \int \rho(z, \omega)\, d\omega, \tag{7}$$

and use this result to define the orientational distribution function (ODF) $\hat{f}(z, \omega) = \rho(z, \omega)/\rho(z)$, from which we can calculate the orientational order parameters in the laboratory-fixed frame [48]:

$$\eta(z) = \langle P_2(\cos\theta)\rangle = Q_{zz}, \tag{8}$$

$$\varepsilon(z) = \langle \sin 2\theta\, \sin\phi\rangle = \frac{4}{3} Q_{yz}, \tag{9}$$

$$\nu(z) = \langle \sin 2\theta\, \cos\phi\rangle = \frac{4}{3} Q_{xz}, \tag{10}$$

$$\varsigma(z) = \langle \sin^2\theta\, \cos 2\phi\rangle = \frac{2}{3}(Q_{xx} - Q_{yy}), \tag{11}$$

$$\tau(z) = \langle \sin^2\theta\, \sin 2\phi\rangle = \frac{4}{3} Q_{xy}, \tag{12}$$

where $\langle \mathcal{A}\rangle = \int \mathcal{A}\hat{f}(z, \omega)\, d\omega$. These equations allow us to write down the five independent components of the nematic order parameter tensor, $Q_{\alpha\beta} = \langle \frac{1}{2}(3\hat{\omega}_\alpha\hat{\omega}_\beta - \delta_{\alpha\beta})\rangle$, in terms of the order parameters in the laboratory-fixed frame:

$$Q_{xx} = -\frac{1}{2}\,\eta + \frac{3}{4}\,\varsigma, \tag{13}$$

$$Q_{yy} = -\frac{1}{2}\,\eta - \frac{3}{4}\,\varsigma, \tag{14}$$

$$Q_{zz} = \eta, \tag{15}$$

$$Q_{xy} = \frac{3}{4}\,\tau, \tag{16}$$

$$Q_{yz} = \frac{3}{4}\,\varepsilon, \tag{17}$$

$$Q_{xz} = \frac{3}{4}\,\nu. \tag{18}$$

$Q_{\alpha\beta}$ give the fraction of molecules oriented along the z-axis (Q_{zz}); along the bisectors of the yz-, xz- and xy-quadrants (Q_{yz}, Q_{xz} and Q_{xy}, respectively); and the difference between the fractions of molecules oriented along the x- and y-axes ($Q_{xx} - Q_{yy}$).

In an earlier paper [30], we characterised the overall nematic order (both uniaxial and biaxial) and the biaxial order of the film using the two scalar order parameters q and β^2 [30, equations (19) and (20)], originally proposed by Hess [49]. However, in the present work we found that β^2 is very noisy when $\mathrm{Tr}\mathbf{Q} \sim 0$, i.e., in weakly-ordered regions, which may

obscure any truly biaxial behaviour. As we shall see in section IV, the **Q** tensor we obtain, be it from theory or from simulation, is almost always approximately diagonal, hence it is appropriate to characterise biaxiality using $Q_{xx} - Q_{yy}$ instead.

III. SIMULATIONS

To find the phase diagram of oblate HGOs, we ran 10 different bulk NVT MC simulation sequences, for particles with length-to-breadth ratios $\kappa = 0.05$, 0.1, 0.15, 0.2, 0.25, 0.3, 0.345, 0.35, 0.4 and 0.45. All simulations were performed using $N = 864$ particles. Periodic boundary conditions were applied in all three directions. The simulation box height was set to $L_Z = 6\sigma_0$ and kept constant during each simulation sequence. The simulation box lengths in the other directions were determined, for each imposed value of the dimensionless, or reduced, number density $\rho^* = \rho\sigma_0^3$, by the relationship $L_x = L_y = (N\sigma_0^3/\rho^* L_z)^{1/2}$. Each system studied was compressed from the isotropic phase ($\rho^* = 1.5$) into the nematic density range by increasing the number density by $\delta\rho^* = 0.1$ after each run. At each density, run lengths of one million MC sweeps (where one sweep represents one attempted move per particle) were performed, averages being accumulated for the final 500 000 sweeps. The phases can be characterised partly through the long-range orientational order of the particles. Ideally, this order parameter should equal zero for an isotropic distribution of particle orientations and one for a perfectly-aligned phase. We define P_2 as the nematic order parameter: it is the average over all particles of the second Legendre polynomial in $\cos\alpha$, where α is the angle between the (in the case of oblates) short particle axis and the nematic director **n**:

$$P_2 = \langle P_2(\cos\alpha)\rangle = \left\langle \frac{3}{2}\left(\cos^2\alpha \frac{1}{2}\right)\right\rangle . \tag{19}$$

P_2 was calculated as an average of 500 values for each reduced density ρ^* during the production run of each simulation. From these, the density at which the I–N phase transition occurs for each κ could be determined. Figure 2 plots P_2 *vs* ρ^* for five representative particle elongations. Because P_2 is a continuous function of ρ^*, we resort to two approximate methods to find the I–N coexistence densities, ρ_I^* and ρ_N^*, as described below. These methods are illustrated in figure 3, where we chose $\kappa = 0.1$ for clarity of presentation only.

Method 1: For each κ, we fit the P_2 data in the lower and higher reduced density ranges to straight lines (shown as solid blue lines in the top panel of figure 3). Then ρ_I^* (ρ_N^*) is

defined as the highest (lowest) reduced density for which P_2 remains within 5% of its lower- (upper-) density-range linear fit. As can be seen from the snapshots in figure 3, the system is uniformly isotropic in the lower-density linear range, clearly nematic in the upper-density linear range, and comprises a mixture of isotropic and nematic domains in the intermediate-density range.

Method 2: We use the fact that the distribution of P_2 should be Gaussian in any one-phase region (except when disordered, since P_2 cannot be negative), but not in a two-phase region. We use the skewness of the distribution, which is based on its third moment about the mean, as a measure of deviation from Gaussian behaviour: for each κ we construct the histograms of P_2 at all densities simulated and compute the skewness as follows:

$$\text{Skewness} = \sum_i w_i^{3/2} z_i^3 \frac{N_w}{(N_w - 1)(N_w - 2)}, \tag{20}$$

where $z_i = (x_i - \bar{x})/s$, w_i is the weight of the ith value, s the weighted standard deviation, $\bar{x}$ is the weighted mean of the values and N_w is the number of weights that are non-zero. We then identify ρ_I^* as the density at which the gradients of both P_2 and the skewness are positive and maximal, and ρ_N^* as the highest density above ρ_I^* for which the skewness is negative. See the bottom panel in figure 3.

The resultant sets of coexistence densities are plotted, as a function of κ, in figure 4.

The effect of confinement was then studied by performing NVT MC simulations of $N = 864$ HGO particles of length-to-breadth ratio $\kappa = 0.345$, sandwiched between two symmetric substrates a distance $L_z = 6\sigma_0$ apart. Periodic boundary conditions were imposed in the x and y directions. For this system, the bulk (reduced) isotropic and nematic coexistence densities are $\rho_I^* = 2.2$ and $\rho_N^* = 3.0$ (method 1) or $\rho_I^* = 2.2$ and $\rho_N^* = 2.5$ (method 2). Each system was initialised at a low density ($\rho^* = 1.5$) and gently compressed by decreasing the box dimensions L_x and L_y while keeping the substrate separation L_z fixed. Analysis was performed by dividing the stored system configurations into 100 equidistant constant-z slices and, in the production phase, performing averages of relevant observables in each slice. This yields profiles of quantities such as the number density $\rho^*(z)$, from which structural changes can be assessed. Orientational order parameter profiles have also been calculated,

particularly

$$Q_{zz}(z) = \frac{1}{N(z)} \sum_{i=1}^{N(z)} \left(\frac{3}{2} u_{i,z}^2 - \frac{1}{2} \right), \tag{21}$$

which measures the variation across the confined films of orientational order measured with respect to the substrate normal. Here $N(z)$ is the instantaneous occupancy of the relevant slice.

IV. RESULTS

We started by calculating the phase diagram of HGOs, oblate as well as prolate, to check the quality of the Parsons-Lee density re-scaling of Onsager's theory. From the bulk version of equation (2) (i.e., with all spatial integrations extended to $\pm\infty$ and $\mathcal{V}^{HDW}(z,\theta) = 0$), we found the pressure and the chemical potential of the I and N phases and performed the standard double-tangent construction. Both the angle-averaged second virial coefficient (for the I phase) and the angle-dependent excluded volume (for the N phase) are known analytically (see, e.g., [50]). The remaining integrations over ω_i were carried out by 16-point Gauss-Legendre quadrature.

Figure 4 shows the phase diagram, in terms of the packing fraction ξ versus elongation κ. For oblate particles ($\kappa < 1$), the coexistence points were determined from simulation as described in section III; for completeness, we have also included de Miguel and del Rio's Gibbs-Duhem integration results from simulation of prolate particles ($\kappa > 1$) [51]. It is seen that our theory performs systematically better for prolate than oblate HGOs: presumably, this is a consequence of the fact that the virial coefficients of oblate particles decrease more slowly with increasing order than do those of prolate particles. This was originally predicted by Onsager himself [52] and confirmed by the first MC simulations of hard discs [53, 54]. Theory clearly overestimates the I–N transition density for all elongations: e.g., for $\kappa = 0.345$, which was used in our study of the confined fluid, the transition is predicted to occur around $\rho^* \sim 2.9$, whereas simulation gives $\rho^* \sim 2.5$. This shortcoming of the (Parsons-Lee uncorrected) Onsager approximation is consistent with what was originally reported by Schmidt and co-workers for infinitely thin discs (the $\kappa \to 0$ limit of our model) [14]. Moreover, simuation finds that the packing fraction gap between coexisting I and N phases is fairly κ-independent, whereas theory predicts it clearly to decrease as $\kappa \to 1$.

For the confined systems, equation (4) was solved iteratively for $\rho(z,\omega)$ by the Picard

method, with an admixture parameter of 0.9 (i.e., 90% of 'old' solution in each iteration), starting from a uniform and isotropic profile. Following Chrzanowska [55], all integrations were performed by Gauss-Legendre quadrature using 64 z-points (the minimum necessary to resolve the structure of the profiles at the higher densities considered) and 16×16 ω-points (for consistency with the bulk calculation). Convergence was deemed to have been achieved when the error, defined as the square root of the sum of the squared difference between consecutive iterates at $64 \times 16 \times 16 = 16384$ points, was less than 10^{-4}. The density and order parameter profiles were then calculated from equations (7) and (8)–(12), respectively.

All results presented are for $\kappa = 0.345$ and substrate separation $L_z = 6\sigma_0$. Figure 5 shows the reduced density $\rho^*(z)$, order parameter $Q_{zz}(z)$ and biaxiality order parameter $Q_{xx}(z) - Q_{yy}(z)$ for $D_s = 1.0$, corresponding to the most impenetrable substrate case. As might be intuitively expected, and as reported by Reich and Schmidt [17] for infinitely thin disks, the preferred particle alignment is homeotropic, or face-on ($Q_{zz}(z) > 0$) and there is no biaxiality ($Q_{xx}(z) - Q_{yy}(z) \sim 0$). At low densities there are only two density peaks, located $\sim 0.5\sigma_0 = D/2$ from either substrate, corresponding to freely rotating HGOs. As ρ^* is increased, two new density peaks appear, a distance $\sim 0.1\sigma_0$ from either substrate, which eventually grow higher than the original peaks. This is qualitatively the same behaviour as for prolate HGOs between symmetric impenetrable walls [28]. Agreement between theory and simulation begins to deteriorate at a fairly low bulk density ($\rho^* = 1.6$), i.e., substantially lower than that of the bulk I–N transition. At the highest bulk density considered ($\rho^* = 3.1$), theory fails to predict the positions of the first two density peaks at the substrates. At the intermediate bulk density ($\rho^* = 2.5$), the film is ordered according to simulation, but not according to theory (cf. figure 4). At this bulk density, however, our density profiles (from theory as well as simulation) exhibit a rather richer structure than those calculated by Reich and Schmidt for infinitely thin discs at I–N coexistence [17]. Also unlike theirs, our order parameter profiles always reach a maximum (equal to unity) right at the substrates. This is a consequence of the almost trivial fact that a particle with $D_s = 1.0$ can only get arbitrarily close to a substrate by being perfectly face-on aligned.

Figure 6 shows the same quantities for $D_s = 0.0$, corresponding to the maximally-penetrable substrate that excludes only the particles' centres of mass. Now the highest-density peaks occur right at the substrates, and the preferred alignment is planar, or edge-on ($Q_{zz}(z) < 0$). Furthermore, there is strong biaxiality ($|Q_{xx}(z) - Q_{yy}(z)| \gg 0$) at the higher

(N) densities, as the nematic director – the mean direction of the particles' minor axes – adopts one particular orientation in the xy-plane. Unlike for $D_s = 1.0$, at the two lower densities ($\rho^* = 1.6$ and $\rho^* = 2.5$) theory and simulation agree that the system is isotropic. At the highest density ($\rho^* = 3.1$) both theory and simulation show strong layering, but the two approaches give differing numbers of layers: the amplitudes of both the density and the order parameters peaks are underestimated by theory, whereas the density peak spacing is overestimated. This leads to a prediction of only five peaks (against simulation's six) at z-positions that are integer multiples of σ_0, i.e., no layer intercalation.

Clearly there will be a crossover from edge-on to face-on alignment at some value of D_s between 0 and 1. For $D_s = 0.5$ (figure 7) both theory and simulation agree that the first density peaks lie $\sim 0.25\sigma_0 = D/2$ from either substrate and that anchoring is still edge-on. However, whereas theory predicts a rather large biaxiality in the N phase ($\rho^* = 3.1$), none is borne out by simulation. This is a result of strong director fluctuations: although the minor axes of particles are instantaneously aligned along some direction in the xy-plane, that direction itself changes on the scale of a few MC steps, leading to $Q_{xx}(z) - Q_{yy}(z) \sim 0$. In contrast, for $D_s = 0.55$ (figure 8) theory predicts edge-on alignment with biaxiality and very strong layering, whereas simulation yields uniaxial face-on alignment with only very moderate layering close to the substrates. Finally for $D_s = 0.7$ theory and simulation again agree that the preferred alignment is face-on (figure 9). We thus conclude that the crossover from edge-on to face-on anchoring occurs for $0.5 \leq D_s \leq 0.55$, but our theory predicts it for $0.65 \leq D_s \leq 0.7$.

Figure 10 shows snapshots of the simulated systems in figures 5 and 7–9. At the intermediate density $\rho^* = 2.5$, the homeotropic (face-on) films are more strongly aligned than the planar (edge-on) ones: this is consistent with the finding of Piñeiro *et al.* [19] that a first layer of adsorbed edge-on particles at a substrate acts as a rough hard wall for subsequent particles, thus promoting disorder. Interestingly, when the substrates favour edge-on anchoring, we do not see a mismatch between the orientations of the particles' minor axes in the N layers growing at either substrate as the I–N transition is approached, leading to a disclination near the midplane of the film, as reported for oblate GB particles in [21, 24]. This may be because these authors performed MD, rather than MC, simulations, for which the system can get trapped in a dynamically-arrested state.

V. CONCLUSIONS

In this paper we have presented a combined MC simulation and DFT treatment of an oblate HGO particle fluid confined between identical parallel substrates. The anchoring can be tuned by varying the extent to which a particle is allowed to penetrate the substrates. The Onsager approximation, combined with a simple Parsons-Lee density re-scaling, previously applied to confined prolate HGO particle fluids, can in some cases yield semi-quantitative predictions for (i) the bulk phase diagram, and (ii) the density and orientational distribution for elongations as large as $\kappa = 0.345$. Many of our density profiles exhibit fairly strong oscillations, which are indicative of layering phenomena and are expected if the density is not very low, i.e., deeper into the N phase than the immediate vicinity of the I–N transition. However, we find no clear evidence of columnar phases at the densities investigated. This is consistent with the fact that no translationally-ordered mesophases of hard ellipsoids have been observed to date [2].

So far we have considered only symmetric confinement, i.e., where the two substrates induce the same type of anchoring. It is nevertheless straightforward to generalise this to hybrid confinement, by allowing the substrates to have different enough penetrabilities. As is the case with prolate HGOs [27, 29, 30], hybrid oblate HGO films will exhibit much richer structures, and may be technologically more relevant. This work is in progress and will be published elsewhere.

Although our theory is qualitatively reliable, quantitatively it performs rather more poorly for oblate than for prolate paticles. We are currently implementing the more accurate Schmidt's FM-DFT [14] of infinitely-thin hard discs for our particular choice of substrates.

Acknowledgments

We acknowledge financial support from the Portuguese Foundation for Science and Technology (FCT) under Contracts nos. UIDB/00618/2020 and UIDP/00618/2020. and from

Instituto Politécnico de Lisboa under project IPL/2019/DISCONEDGE_ISEL.

[1] Allen MP. Molecular simulation and theory of liquid crystal surface anchoring. Mol Phys. 1999;96:1391–1397.

[2] Allen MP. Molecular simulation of liquid crystals. Mol Phys. 2019;117:2391–2417.

[3] de las Heras D, Velasco E, Mederos L. Capillary smectization and layering in a confined liquid crystal. Phys Rev Lett. 2005;94:017801.

[4] de las Heras D, Velasco E, Mederos L. Capillary effects in a confined smectic phase of hard spherocylinders: Influence of particle elongation. Phys Rev E. 2006;74:011709.

[5] Semiromi MA, Avazpour A. Anchoring transition of confined prolate hard spherocylinder liquid crystals: hard needle-wall potential. Liq Cryst. 2018;45:1396–1407.

[6] Collings PJ. Liquid Crystals: Nature's Delicate Phase of Matter, 2nd edition. Princeton (NJ): Princeton University Press; 2001.

[7] Tschierske C. Micro-segregation, molecular shape and molecular topology – partners for the design of liquid crystalline materials with complex mesophase morphologies. J Mater Chem. 2001;11:2647–2671.

[8] van der Kooij FM, Lekkerkerker HNW. Formation of Nematic Liquid Crystals in Suspensions of Hard Colloidal Platelets. J Phys Chem B. 1998;102:7829–7832.

[9] Pizzey C, van Duijneveldt JS, Klein S. Liquid Crystal Clay Composites. Mol Cryst Liq Cryst 2004;409:51–57.

[10] Zou C, Wang J, Wang M, Wu Y, Gu K, Shen Z, Xiong G, Yang H, Jiang L, Ikeda T. Patterning of discotic liquid crystals with tunable molecular orientation for electronic applications. Small. 2018;14:1800557.

[11] Bushby RJ, Kawata K. Liquid crystals that affected the world: discotic liquid crystals. Liq Cryst. 2011;38:1415–1426.

[12] Harnau L, Dietrich S. Fluids of platelike particles near a hard wall. Phys Rev E. 2002;65:021505.

[13] Harnau L, Dietrich S. Wetting and capillary nematization of binary hard-platelet and hard-rod fluids. Phys Rev E. 2002;66:051702.

[14] Esztermann A, Reich H, Schmidt, M. Density functional theory for colloidal mixtures of hard

platelets, rods, and spheres(2006). Phys Rev E. 2006;73:011409.

[15] van der Beek D, Reich H, van der Schoot P, Dijkstra M, Schilling T, Vink R, Schmidt M, van Roij R, Lekkerkerker H. Isotropic-nematic interface and wetting in suspensions of colloidal platelets. Phys Rev Lett. 2006;97:087801.

[16] Reich H, Dijkstra M, van Roij R, Schmidt M. Entropic Wetting and the Free Isotropic-Nematic Interface of Hard Colloidal Platelets (2007). J Phys Chem B. 2007;111:7825–7835.

[17] Reich H, Schmidt M. Capillary nematization of hard colloidal platelets confined between two parallel hard walls. J Phys: Condens Matter. 2007;19:326103.

[18] Kapanowski A, Abram M. Model of hard spheroplatelets near a hard wall. Phys Rev E. 2014;89:062503.

[19] Piẽiro MM, Galindo A, Parry AO. Surface ordering and capillary phenomena of confined hard cut-sphere particles. Soft Matter. 2007;3:768–778.

[20] Avendaño C, Jackson G, Wensink HH. Nanorings in planar confinement: the role of repulsive surfaces on the formation of lacuna smectics. Mol Phys. 2018;116:2901–2910.

[21] Bellier-Castella L, Caprion D, Ryckaert J-P. Surface ordering of diskotic liquid crystals. J Chem Phys. 2004;121:4874-4883.

[22] Caprion D. Discotic molecules in cylindrical nanopores: A Monte Carlo study. Eur Phys J E. 2009;28:305–313.

[23] Busselez R, Cerclier CV, Ndao M, Ghoufi A, Lefort R, Morineau D. Discotic columnar liquid crystal studied in the bulk and nanoconfined states by molecular dynamics simulation. J Chem Phys. 2014;141:134902.

[24] Salgado-Blanco D, Mendoza CI, Chvez-Rojo MA, Moreno-Razo JA, Daz-Herrera E. Influence of anchoring in the phase behaviour of discotic liquid crystals. Soft Matter. 2019;14:2846–2859.

[25] Salgado-Blanco D, Daz-Herrera E, Mendoza CI. Effect of the anchoring strength on the phase behaviour of discotic liquid crystals under face-on confinement. J Phys: Condens Matter. 2019;31:105101.

[26] Chrzanowska A, Teixeira PIC, Eherentraut H, Cleaver DJ, Ordering of hard particles between hard walls. J Phys: Condens Matter. 2001;13:4715–4726.

[27] Cleaver DJ, Teixeira PICT. Discontinuous structural transition in a thin hybrid liquid crystal film. Chem Phys Lett. 2001;338:1–6.

[28] Teixeira PIC, Barmes F, Cleaver DJ. Symmetric alignment of the nematic matrix between

close penetrable colloidal particles. J Phys: Condens Matter. 2004;16:S1969–S1980.

[29] Teixeira PIC, Barmes F, Anquetil-Deck C, Cleaver DJ. Simulation and theory of hybrid aligned liquid crystal films. Phys Rev E. 2009;79:011709.

[30] Teixeira PIC. Nematic liquid crystal order reconstruction in ultraconfinement, from density-functional theory. Liq Cryst. 2016;43:1526–1535.

[31] Rigby M. Hard Gaussian overlap fluids. Mol Phys. 1989;68:687–697.

[32] Perram JW, Wertheim MS. Statistical mechanics of hard ellipsoids: 1. Overlap algorithm and the contact function. J Comput Phys. 1985;58:409–416.

[33] Allen MP, Evans GT, Frenkel D, Mulder BM. Hard convex body fluids. Adv Chem Phys. 1993;86:1–166.

[34] Perram JW, Rasmussen J, Praestgaard E, Lebowitz JL. Ellipsoid contact potential: Theory and relation to overlap potentials. Phys Rev E. 1996;54:6565–6573.

[35] Bhethanabotla VR, Steele W. A comparison of hard-body models for axially-symmetrical molecules. Mol Phys. 1987;60:249–251.

[36] Huang SL, Bhethanabotla VR. Virial coefficients for the Hard Gaussian Overlap model. Int J Mod Phys C. 1999;10:361–374.

[37] Velasco E, Mederos L. A theory for the liquid-crystalline phase behavior of the Gay-Berne model. J Chem Phys. 1998;109:2361–2370.

[38] Anquetil-Deck C, Cleaver DJ, Bramble JP, Atherton TJ. Independent control of polar and azimuthal anchoring. Phys Rev E. 2013;88:012501.

[39] DeBenedictis A, Atherton TJ, Anquetil-Deck C, Cleaver DJ, Emerson DB, Wolak M, Adler JM. Competition of lattice and basis for alignment of nematic liquid crystals. Phys Rev E. 2015;92: 042501.

[40] Evans R. Nature of the liquid-vapor interface and other topics in the statistical mechanics of nonuniform classical fluids. Adv Phys. 1979;28:143–200.

[41] Poniewierski A. Ordering of hard needles at a hard wall. Phys Rev E. 1993;47:3396–3403.

[42] Parsons JD. Nematic ordering in a system of rods. Phys Rev A 1979;19:1225–1230.

[43] Lee SD. A numerical investigation of nematic ordering based on a simple hard-rod model. J Chem Phys. 1997;78:4972–4874.

[44] Somoza AM, Tarazona P. Density functional approximation for hard-body liquid crystals. J Chem Phys. 1989;91:517–527.

[45] Velasco E, Mederos L, Sullivan DE. Density-functional theory of inhomogeneous systems of hard spherocylinders. Phys Rev E. 2000;62:3708–3718.

[46] de las Heras D, Mederos L, Velasco E. Wetting properties of a hard-spherocylinder fluid on a substrate. Phys Rev E. 2003;68:031709.

[47] de las Heras D, Velasco E, Mederos L. Effects of wetting and anchoring on capillary phenomena in a confined liquid crystal. J Chem Phys. 2004;120:4949–4957.

[48] Telo da Gama MM. The interfacial properties of a model of a nematic liquid-crystal .2. Induced orientational order and wetting transitions at a solid-fluid interface. Mol Phys. 1984;52:611–630.

[49] Kaiser P, Wiese N, Hess S. Stability and instability of an uniaxial alignment against biaxial distortions in the isotropic and nematic phases of liquid crystals. J Non-Equilib Thermodyn. 1992;17:153–169.

[50] Velasco E, Somoza AM, Mederos L, Liquid crystal phase diagram of the Gay-Berne fluid by perturbation theory. J Chem Phys. 1995;102:8107–8113.

[51] de Miguel E, Martín del Rio E. The isotropic-nematic transition in hard Gaussian overlap fluids. J Chem Phys. 2001;115:9072–9083.

[52] Onsager L. The effects of shape on the interaction of colloidal particles. Ann NY Acad Sci. 1949;51:627–659.

[53] Frenkel D, Eppenga R. Monte Carlo study of the isotropic-nematic transition in a fluid of thin hard disks. Phys Rev Lett. 1982;49:1089–1092.

[54]) Eppenga R, Frenkel D. Monte Carlo study of the isotropic and nematic phases of infinitely thin hard platelets. Mol Phys. 1984;52:1303–1334.

[55] Chrzanowska A. Application of Gaussian quadratures to density functional (df) theories of confined liquid crystals. J Comput Phys. 2003;191:265–281.

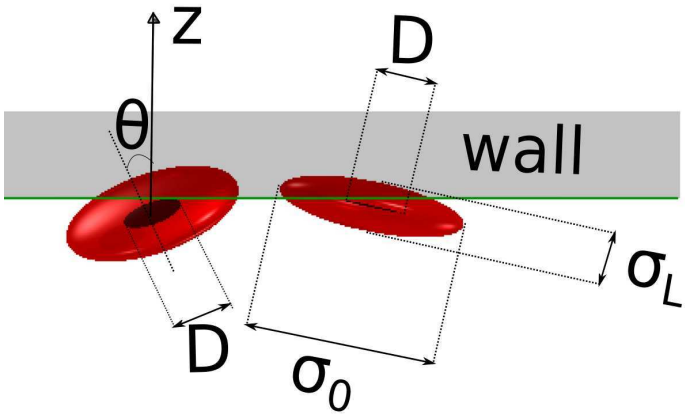

FIG. 1: The HDW potential: the wall sees a particle as a hard disc of diameter D, which need not equal σ_0 Varying D between 0 and σ_0 is equivalent to changing the degree of side-group penetrability into the confining substrates, and hence the substrate's anchoring properties.

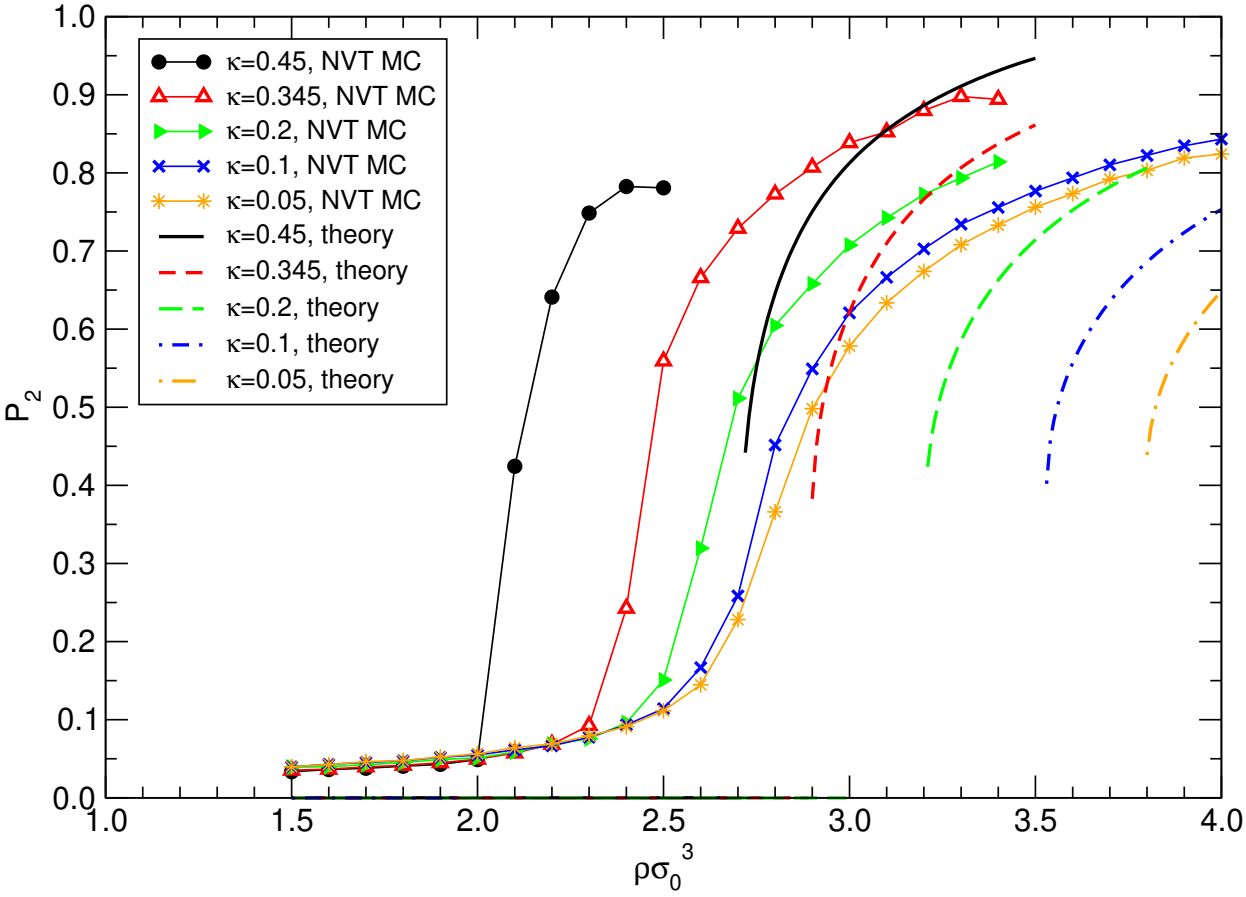

FIG. 2: P_2 *vs* $\rho^* = \rho\sigma_0^3$ from NVT MC simulation (lines with symbols) and theory (lines without symbols), for a few particle elongations. Simulation results show a continuous variation, whereas the theory curves exhibit a jump at the first-order I–N transition.

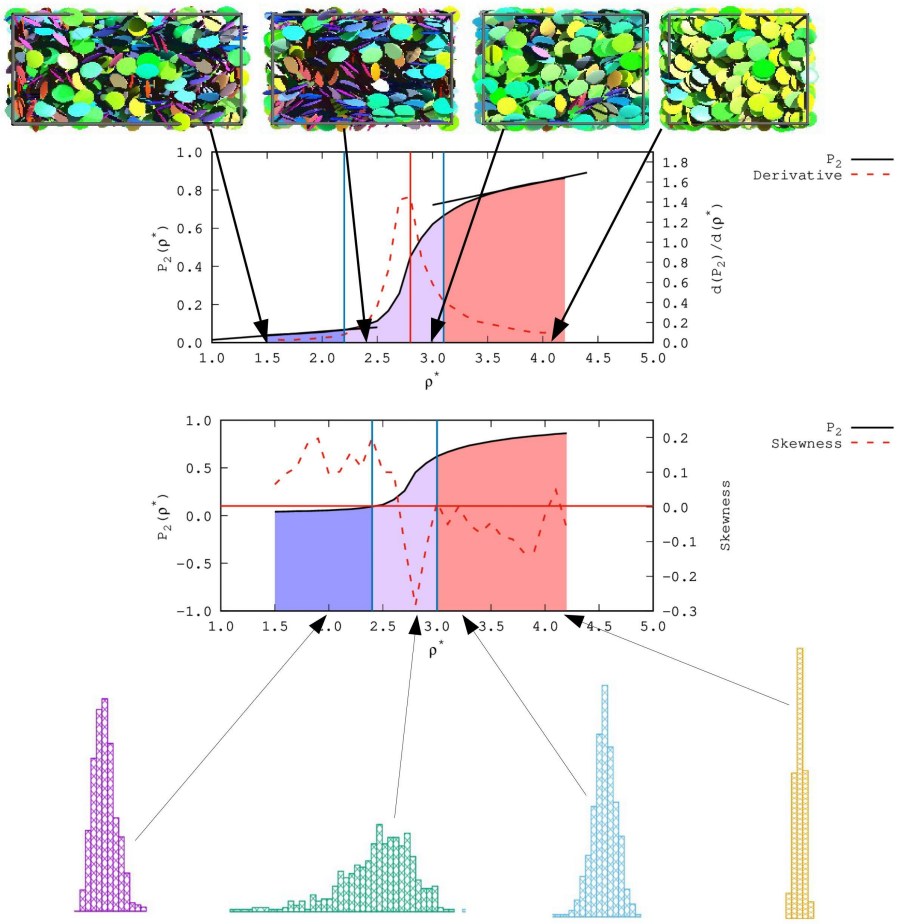

FIG. 3: Illustration of the two methods used to find the coexisting I and N densities from NVT MC data. For clarity we choose $\kappa = 0.1$ and plot P_2 *vs* $\rho^* = \rho\sigma_0^3$ (solid black lines). In the top panel (*method 1*), the dashed red line is the numerical $dP_2/d\rho^*$ and the blue straight lines are linear fits in the low (left) and high (right) density ranges. Included are also snapshots of typical configurations in each range (top panel), as well as of the P_2 distribution (bottom panel). In the bottom panel (*method 2*), the dashed red line is the skewness. In both panels, the low-density (I) range is shaded blue, the high-density (N) range is shaded pink, and the intermediate-density (I–N) range is shaded purple. See the text for details.

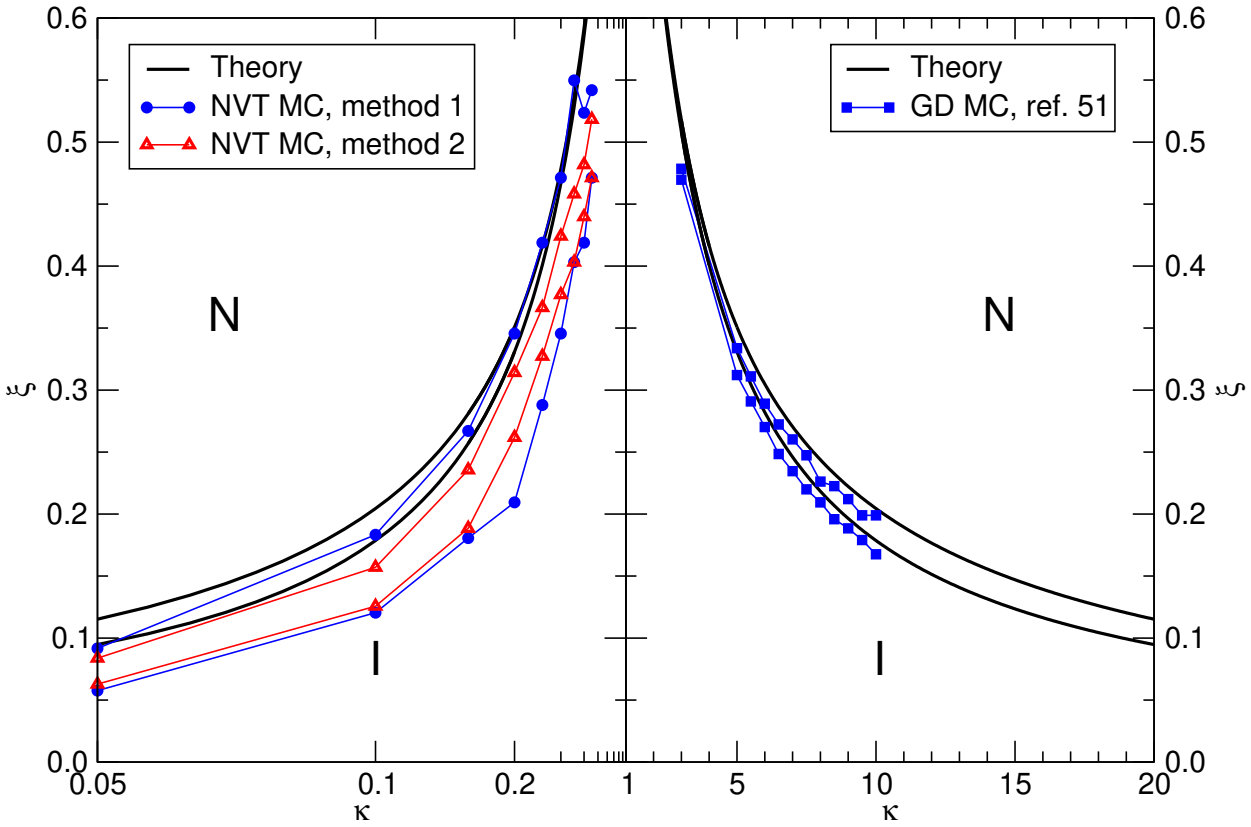

FIG. 4: I–N phase diagram of the HGO fluid: $\xi = \rho v_0 = (\pi/6)\kappa\rho\sigma_0^3$ and κ are the packing fraction and the particle elongation, respectively. The thin lines connecting the symbols are just to guide the eye.

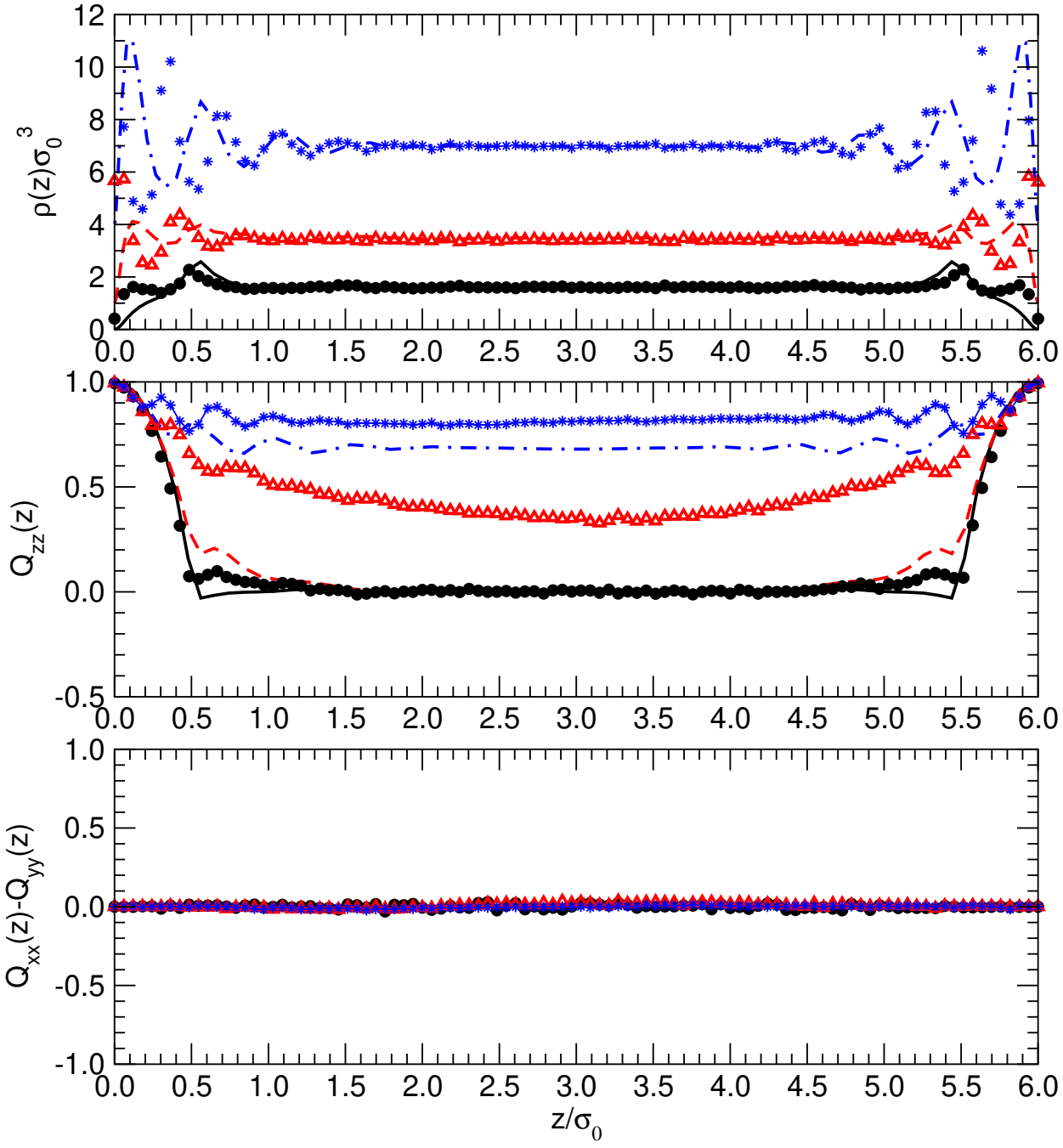

FIG. 5: Reduced density $\rho^*(z)$ (top), order parameter $Q_{zz}(z)$ (middle), and biaxiality order parameter $Q_{xx} - Q_{yy}$ (bottom) profiles from DFT (lines) and simulation (symbols), for a symmetric film of HGO particles of elongation $\kappa = 0.345$ and inner disc diameter $D_s = 1.0$, for reduced bulk densities $\rho^* = 1.6$ (solid line and filled circles), 2.5 (dashed line and open triangles), and 3.1 (dot-dashed line and stars). The lowest density lies in the I phase, the intermediate density in the I–N transition region, and the highest density in the N phase. In the top panel, the data for $\rho^* = 2.5$ and $\rho^* = 3.1$ have been shifted upwards by 1 and 4 units, respectively, for better readability.

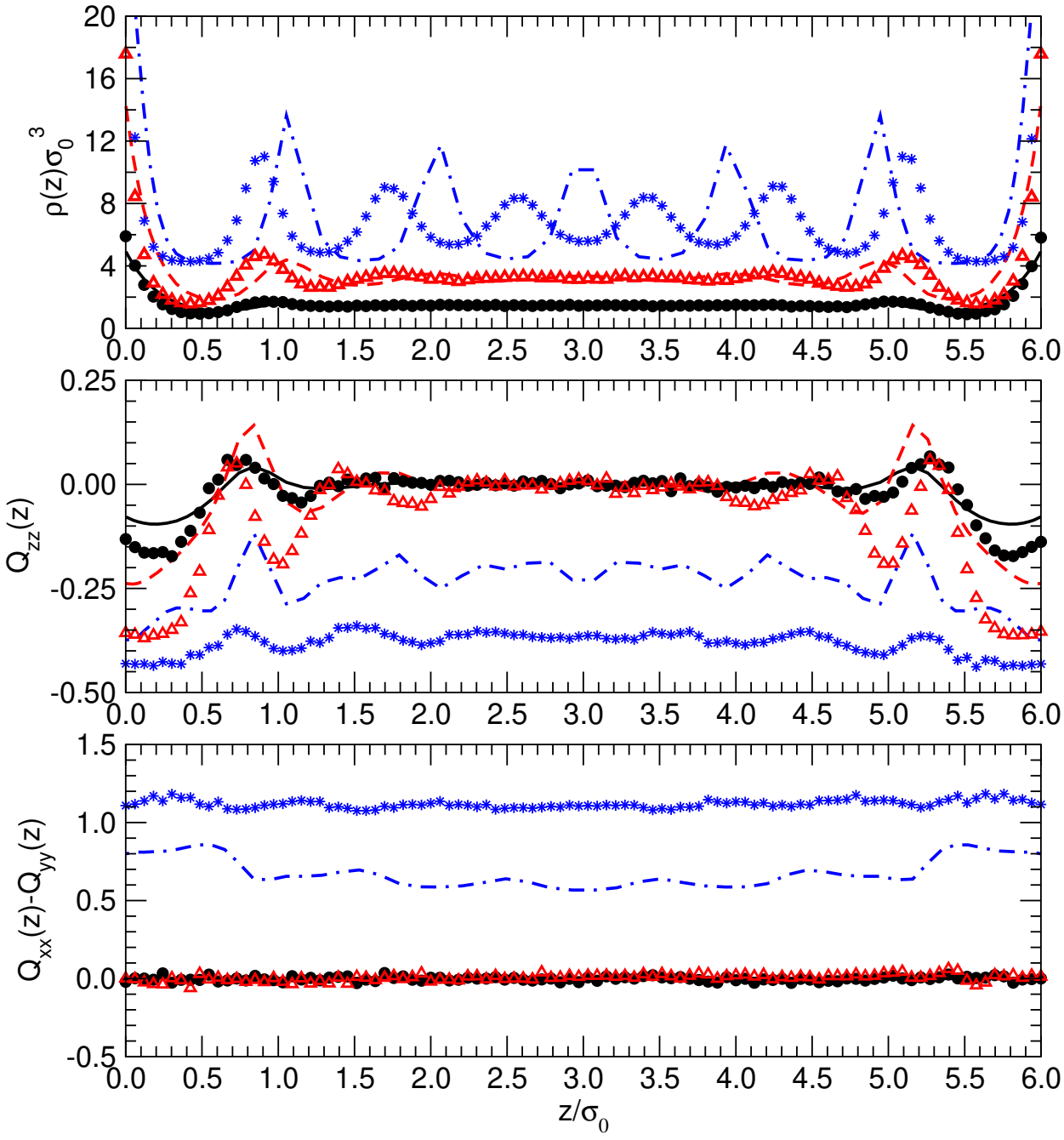

FIG. 6: Same as figure 5, but for $D_s = 0.0$

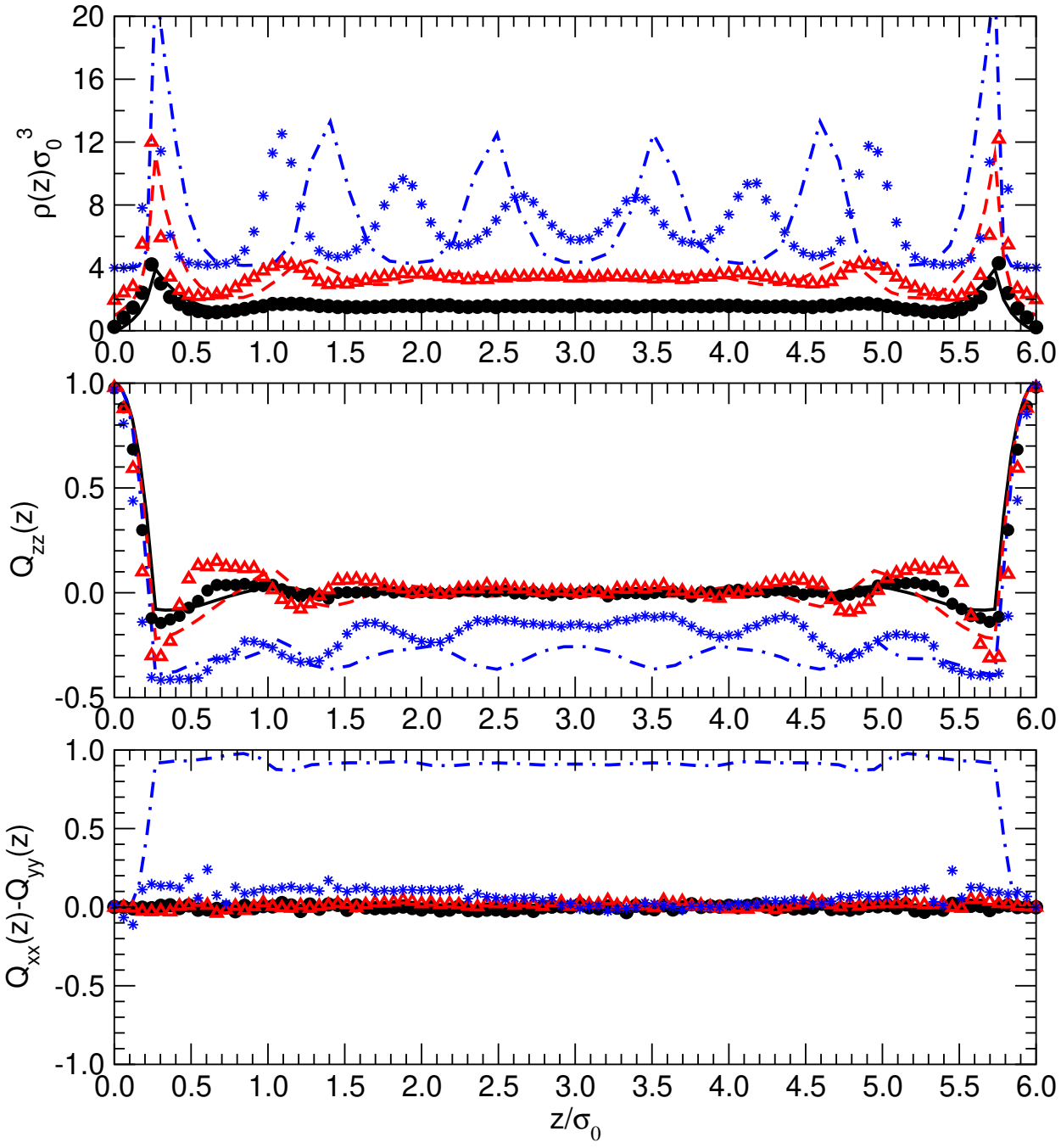

FIG. 7: Same as figure 5, but for $D_s = 0.5$

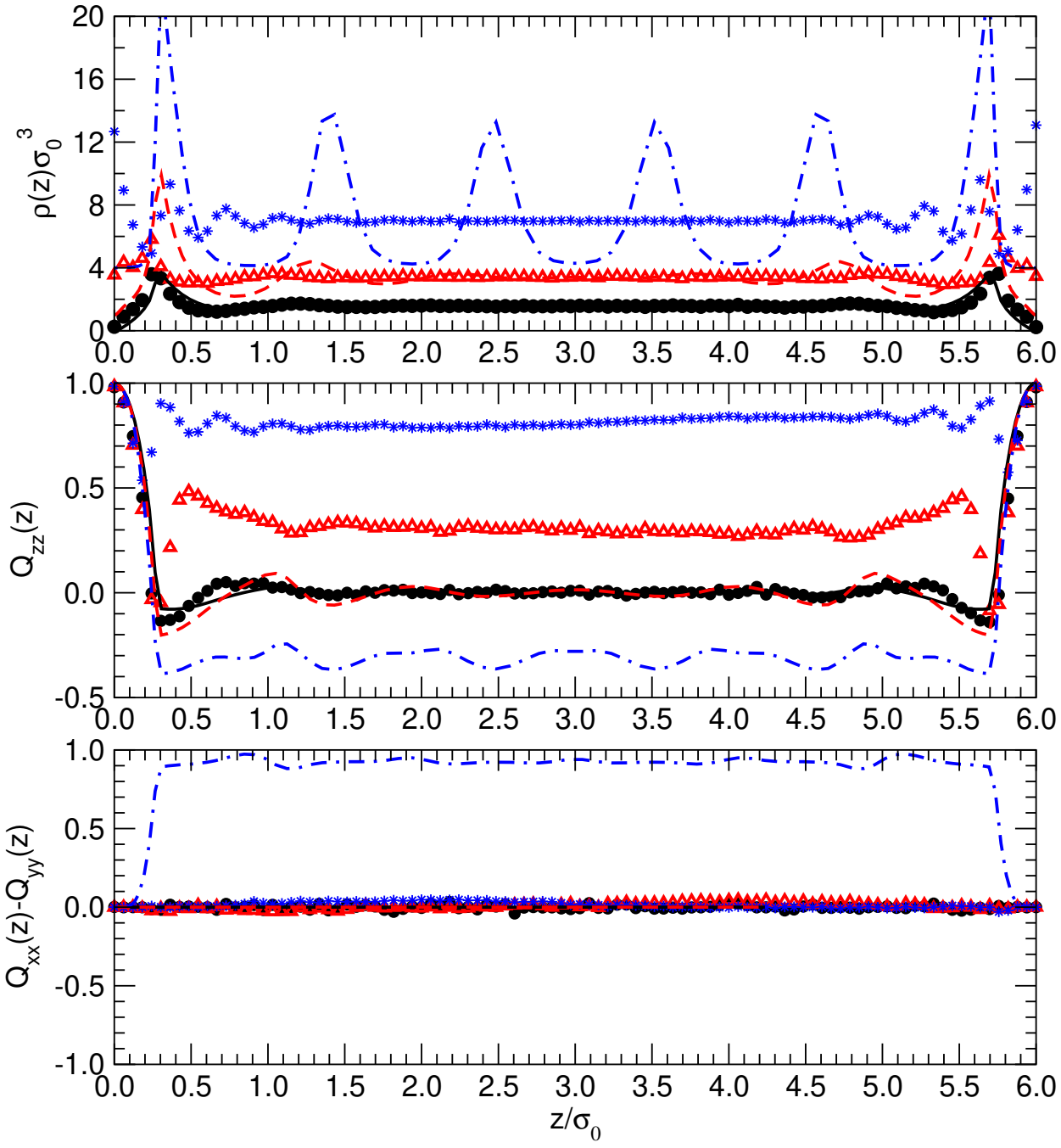

FIG. 8: Same as figure 5, but for $D_s = 0.55$

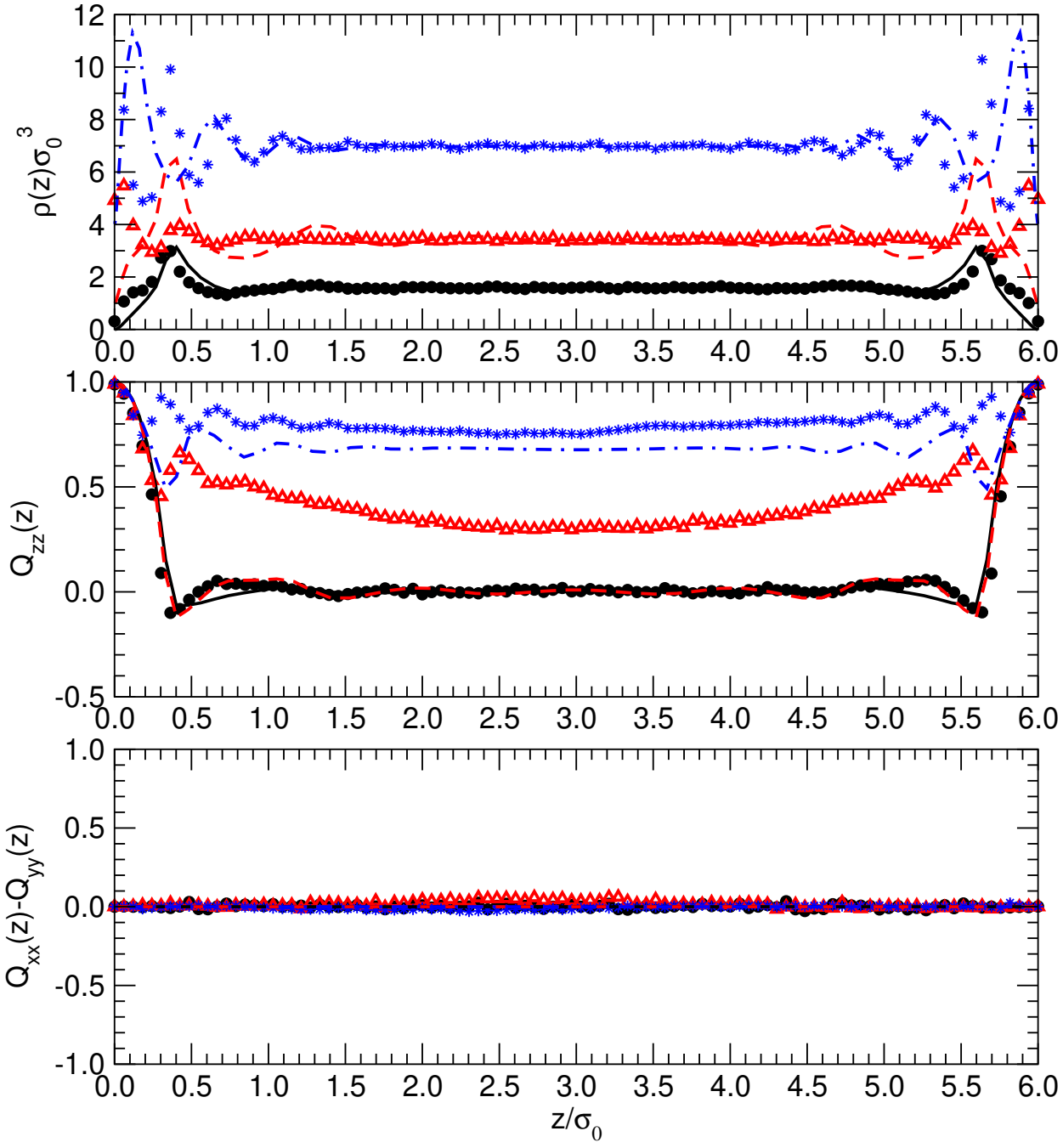

FIG. 9: Same as figure 5, but for $D_s = 0.7$

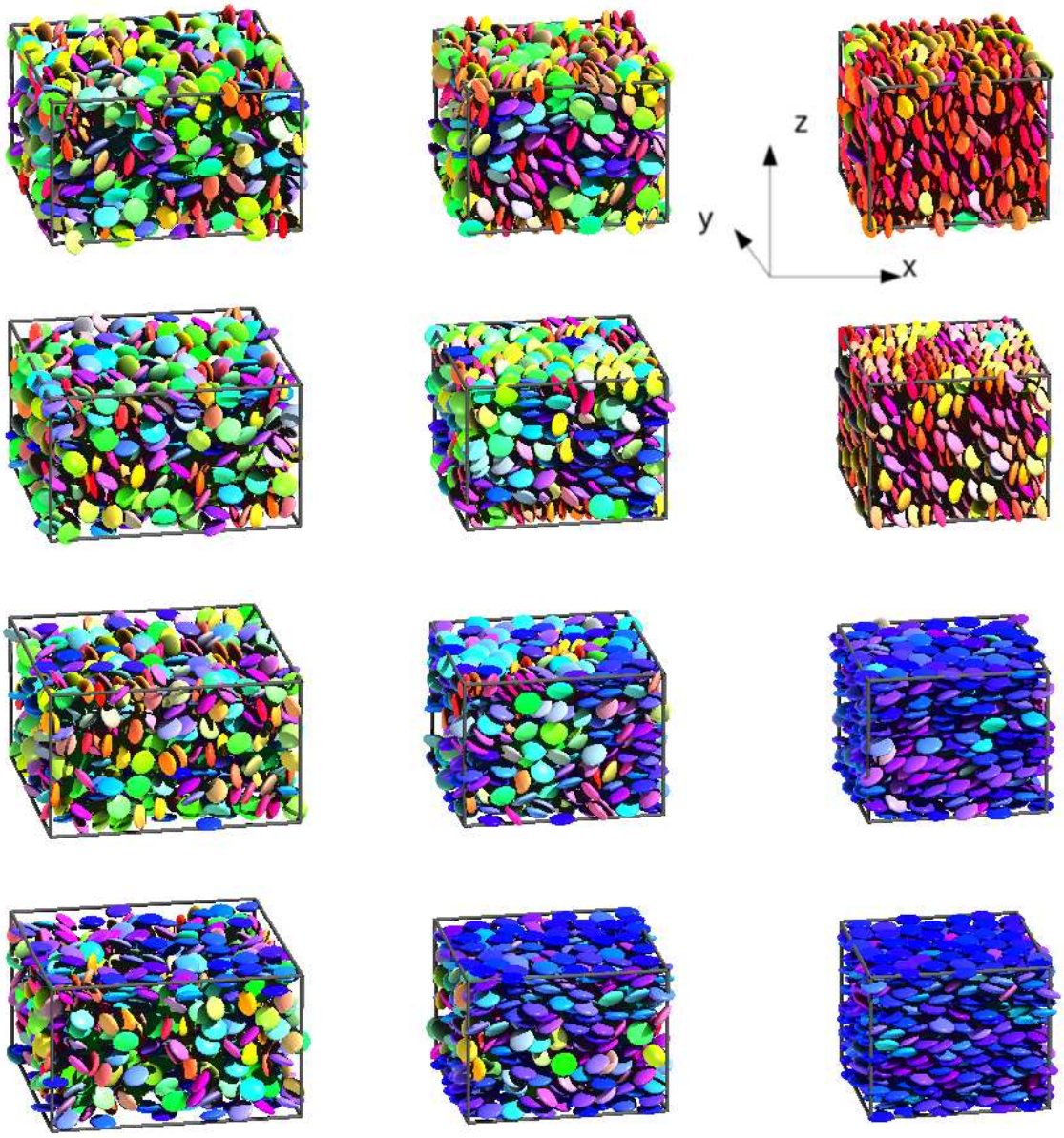

FIG. 10: Configuration snapshots of symmetrically-confined oblate HGO films. First row: $D_s = 0.0$; second row: $D_s = 0.5$; third row: $D_s = 0.55$; fourth row: $D_s = 1.0$. Left column: $\rho^* = 1.6$ (I); middle column; $\rho^* = 2.5$ (I+N); right column: $\rho^* = 3.1$ (N). The substrates (not shown) are at the top and bottom box faces. Colours give the orientation of a particle's short axis: along x (red), along y (green), or along z (blue).